Supplementary Information

The Effect of Atomic Nitrogen on the C_{60} Cage

Hidefumi Nikawa,[†] Yasuyuki Araki,[‡] Zdenek Slanina,[†] Takahiro Tsuchiya,[†] Takeshi Akasaka,*[,†] Takehiko Wada,[‡] Osamu Ito,[‡] Klaus-Peter Dinse,[#] Masafumi Ata,[¶] Tatsuhisa Kato,[%] & Shigeru Nagase[§]

† Center for Tsukuba Advanced Research Alliance, University of Tsukuba, 1-1-1 Tennodai, Tsukuba, Ibaraki 305-8577, Japan.
‡ Institute of Multidisciplinary Research for Advanced Materials, Tohoku University, Sendai, Miyagi 980-8577, Japan.
¶ Technology Information Department, National Institute of Advanced Industrial Science and Technology (AIST) and Headquarters. Office, Ministry of Economy, Trade and Industry, 1-3-1 Kasumigaseki, Chiyodaku, Tokyo 100-8921, Japan.
 # Physical Chemistry III, Darmstadt University of Technology, Petersenstrasse 20, D-64287 Darmstadt, Germany.
% Department of Chemistry, Josai University, Sakado 171-8501, Japan.
§ Department of Theoretical and Computational Molecular Science, Institute for Molecular Science, Okazaki 444-8585, Japan.

Table of contents

Experimental details.

Experimental details

$N@C_{60}$ was prepared by the nitrogen bombardment method and successfully isolated from a crude mixture of $N@C_{60}$, C_{60} , $C_{60}O$, and so on using a multi-step and recycling HPLC system. HPLC was performed by a Cosmosil Buckyprep column (ϕ 20 × 250 mm) and toluene as eluent at a flow rate of 9.9 mL/min at room temperature (Figure S1a, b). To clarify the location of $N@C_{60}$ in the chromatogram, the C_{60} peak was divided into four fractions and each fractions were masured by electron paramagnetic resonance (EPR) measurements using ϕ5mm quart tube (Figure S1c). The volume of EPR sample and concentration of C_{60} for each fraction was 200 μL and 1g/L, respectively. Figure S1a shows the HPLC diagram of our fullerene sample after preparation by nitrogen bombardment method. The vertical lines define the different fractions in which the C_{60} peak was divided (Figure S1b). In Figure S1c, the EPR spectra of the fractions I to IV are displayed. The triplet seen in the lower three spectra is the fingerprint of $N@C_{60}$; the intensity (peak-to-peak height) is a direct measure of the amount of $N@C_{60}$ in the sample. The highest intensity is found in the third fraction, i.e. at the upper tail of the C_{60} peak. Thus $N@C_{60}$ is clearly delayed in our column, compared to C_{60}, and enrichment is possible. Consequently, this preparative HPLC was repeated tens of times for the enrichment of $N@C_{60}$. Finally, several tens of μg $N@C_{60}$ was isolated by recycling HPLC system.

The EPR measurements were performed with a conventional continuous wave spectrometer in the X band (about 9:4 GHz). Figure 2 shows the three characteristic ^{14}N EPR lines (g = 2.0028, hfc = 5.67 G) of the sample irradiated with ^{14}N atom (nuclear spin I = 1, NA = 99.634%) and the doublet ^{15}N EPR lines (g = 2.0028, hfc = 7.96 G) from the sample irradiated with ^{15}N atom (nuclear spin I =1/2, NA = 0.366%). The line splitting is due to the hyperfine interaction with the nuclear spin.

Figure S3-S6 show the decay kinetics of exited states of Ar-saturated toluene solutions of $N@C_{60}$, $N@C_{60}/C_{60}$(3:2), and C_{60} at room temperature. These spectra demonstrated that the presence of the N atom enhances the intrinsic first order decay of $(N@C_{60})^*$. Meanwhile, these decay times are influenced a great deal by the concentration of residual oxygen in the solution, beccase these etxited species are quenched by oxygen. To shed undoubtedly light on the effect of the N atom on C_{60} cage in the exited state, we have performed laser flash photolysis of the deoxygenated toluene solutions of $N@C_{60}$ and C_{60} (Figure S7-S8). The decay rates of the exited states were strongly affected by the laser power as shown in Figure S7 and S8. The decay time profiles are composed of mixed-order kinetics of first- and second-order, in which the former is the intrinsic decay rate of the exited state and the latter is due to the annihilation process among the exited species such as triplet-triplet annihilation in the case of C_{60}. The decay rates of the exited states were strongly affected by the laser power as shown in Figure S7 and S8. The decay time profiles are composed of mixed-order kinetics of first- and second-order, in which the former is the intrinsic decay rate of the exited state and the latter is due to the annihilation process among the exited species such as triplet-triplet annihilation in the case of C_{60}. As shown in an inset of Figure S7 and S8, plot of Δk_T to ΔA_0 shows a linear correlation. From this slope, an intrinsic first-order decay rate (Δk_T^0) of the excited state was estimated.

$^3C_{60}$* is well know to be quenched efficiently by molecular oxygen (O_2) to generate singlet oxygen ($^1O_2$). The quenching of $^3C_{60}$* by molecular oxygen (O_2) is generally probed by monitoring the decrease of the triplet-triplet absorption and the increase of the emission from $^1O_2$ at 1272 nm. The lifetime of $^m(N@C_{60})$* decreased in a O_2-saturated toluene solution and the emission from $^1O_2$ was observed at 1274 nm (Figure S9). This may reveal that $^m(N@C_{60})$* is quenched by triplet oxygen ($^3O_2$) as well as $^3C_{60}$* and the quantum yield (Φ_{ISC}) for formation of $^m(N@C_{60})$* via intersystem crossing from $^{3/2}(N@C_{60})$* was estimated as same as that of $^3C_{60}$* (Φ_{ISC} = 0.96).

The MALDI-TOF MS were measured on a BIFLEXTM III (Bruker, Germany) with 1,1,4,4-tetraphenyl-1,3-butadiene as a matrix. ^{13}C NMR spectra at 125 MHz were measured on a Bruker AVANCE 500 spectrometer with a CryoProbe system in carbon disulfide with a capillary tube of acetone-d_6 as an external lock. UV-vis-NIR spectra were measured on a UV 3150 (Shimadzu, Japan) in toluene. The nanosecond transient absorption spectra were measured by using 532 nm laser light (SHG) of a Nd:YAG laser (Spectra-Physics, Quanta-Ray GCR-130) as an excitation source. A continuous xenon flash lamp was used as a probe light. A Ge-APD module (Hamamatsu Photonics, B2834) attached to a monochromator (Ritsu MC-10N) was employed as a detector of transient absorption spectra in the visible and near-IR regions (400-1000 nm). Emission spectra of the singlet oxygen ($^1O_2$*) in the near-IR regions were detected by using an InGaAs detector. All the spectral measurements were carried out in 1 cm optical cell. All calculations were carried out using the Gaussian 03 program. Geometries were optimized with the hybrid density functional theory at the B3LYP level[i,ii,iii] with the 6-31G(d) basis set[iv] for C and N,

while the chemical shifts were evaluated with the MPW1K functional[v] and the same basis set and calibrated to the observation.[vi]

i) A. D. Becke, *Phys*. *Rev*. A, 1988, **38**, 3098.
ii) A. D. Becke, *J. Chem. Phys*., 1993, **98**, 5648.
iii) C. Lee, W. Yang and R. G. Parr, *Phys*. *R*ev. B, 1988, **37**, 785.
iv) W. J. Hehre, R. Ditchfield and J. A. Pople, *J. Chem*. *Phys*., 1972, **56**, 2257.
v) B. J. Lynch, P. L. Fast, M. Harris and D. G. Truhlar, *J. Phys*. *Chem*. A, 2000, **104**, 4811.
vi) G. Y. Sun and M. Kertesz, *J. Phys*. *Chem*. A 2000, **104**, 7398.

Figure S1.

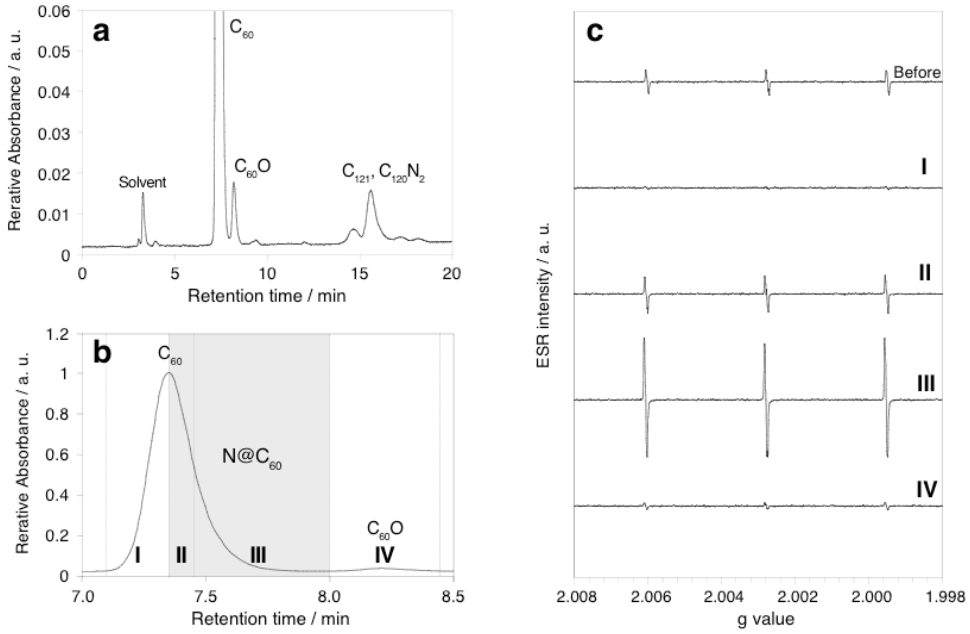

Figure S2.

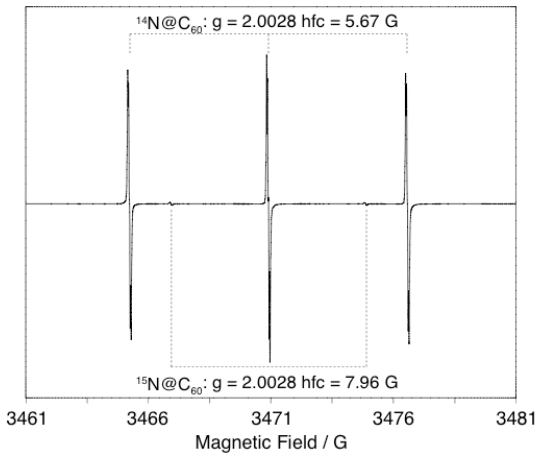

Figure S3.

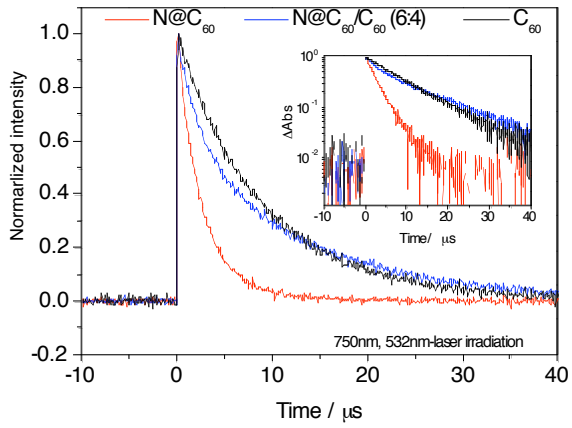

Figure S4.

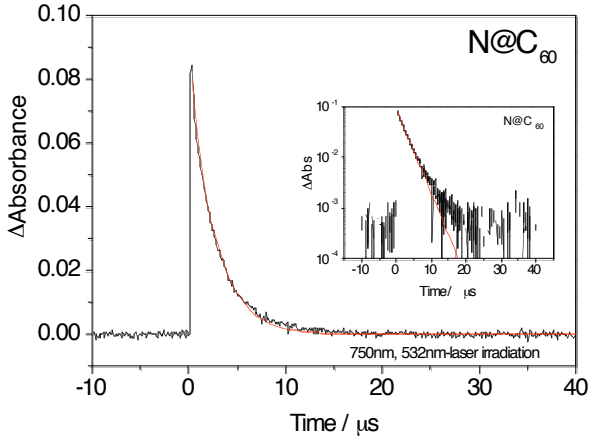

Figure S5.

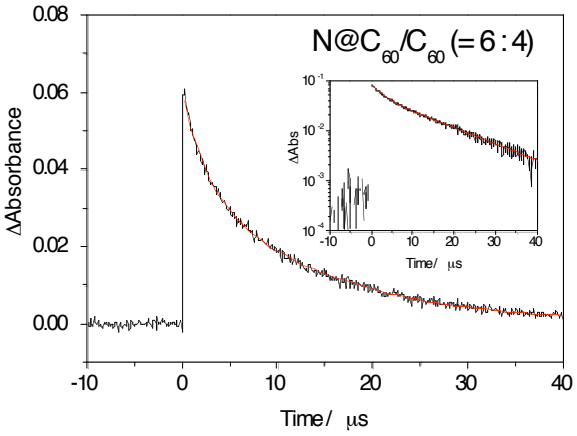

Figure S6.

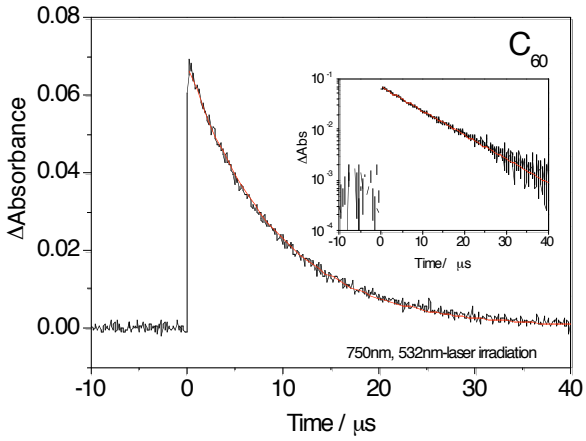

Figure S7.

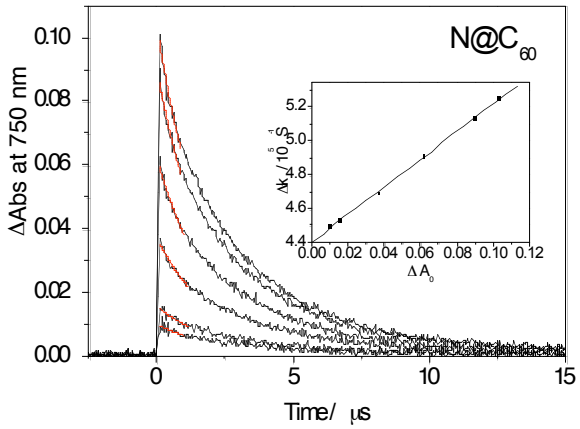

Figure S8.

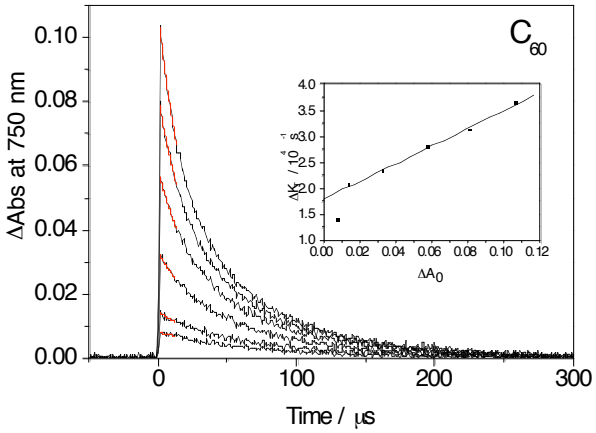

Figure S9.

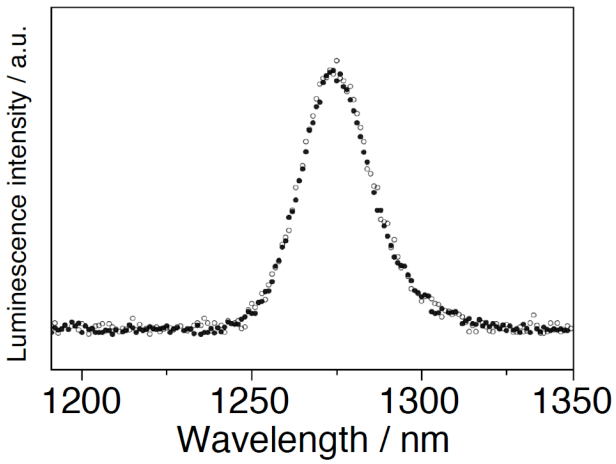
Luminescence intensity / a.u.
1200
1250
1300
1350
Wavelength / nm